McLeod, J.S., et al., 2024, Landscapes on the edge: River intermittency in a warming world: Geology, https://doi.org/10.1130/G52043.1

Supplemental Material

Additional background on climate, extended methodology, and extended intermittency results.

Landscapes on the edge: river intermittency in a warming world

Supplemental Material

Jonah S. McLeod[1,2], Alexander C. Whittaker[1], Rebecca E. Bell[1], Gary J. Hampson[1], Stephen E. Watkins[3], Sam A.S. Brooke[4], Nahin Rezwan[1], Joel Hook[1], Jesse R. Zondervan[5], Vamsi Ganti[6,7], Sinéad J. Lyster[8]

[1]Department of Earth Science and Engineering, Imperial College London, London, UK;

[2]Science and Solutions for a Changing Planet DTP, Grantham Institute, London, UK;

[3]JBA Consulting, UK;

[4]Terrabotics, UK,;

[5]Department of Earth Sciences, University College London, UK;

[6]Department of Geography, University of California Santa Barbara, Santa Barbara, CA, USA;

[7]Department of Earth Science, University of California Santa Barbara, Santa Barbara, CA, USA;

[8]Department of Geosciences, The Pennsylvania State University, State College, PA, USA

S1. Climate projections

The following bibliography is a compilation of studies documenting projected changes in precipitation patterns in the near future across Europe and the Mediterranean. These studies were used to determine an estimated average projected change in extreme precipitation of 20% by 2100. This statistic informs the illustrative example, explained in the main text, that if distributions of extreme rainfall in the Gulf of Corinth are scaled up by 20%, the number of threshold-surpassing flow events would more-than double.

Study area	Projection	Reference
Global	Mean precipitation to reduce, extreme precipitation to increase by 2100	(Goubanova & Li, 2007)
Mediterranean France	10yr return flood to increase in frequency to 2yr return by 2035-65, and the 10yr return flood will carry twice as much water	(Quintana-Seguí et al., 2011)

Greece	Flash floods will increase in magnitude and frequency by 20% by 2050	(Giannakopoulos et al., 2011)
Mediterranean	MAP will decrease, extreme precipitation magnitude will increase	(Miranda et al., 2011)
Europe and Mediterranean	Subdaily maximum rainfall will increase even in regions where MAP decreases	(Westra et al., 2014)
Sardinia	10yr return flood will increase in magnitude by 2070	(Piras et al., 2016)
Europe and Mediterranean	Extreme precipitation will increase by 20% by 2100 in Greece, with a similar trend across the southern Mediterranean, however southern Mediterranean is more variable. RCP4.5 projects a 5-10% increase in the 20yr extreme precipitation by 2100	(Tramblay & Somot, 2018)
Mediterranean	A shift from 22 floods per decade to 28 floods per decade. An increase in extreme events by 27%	(Fang et al., 2022)
Global	Rainfall and flooding will increase by 2080s due to climate change	(He et al., 2022)
Global	Flooding with return 5-100 years could increase 5-50% (CMIP6)	(Meresa et al., 2022)
Algeria	By 2081-2100 MAP will decrease and extreme precipitation will increase	(Sahabi-Abed et al., 2023)

Table S1. Compilation of studies documenting climate projections in Europe and the Mediterranean.

S2: Similar hydroclimates

The studied catchments in Greece are highly intermittent, but their hydroclimate is typical of many rivers across the Mediterranean and worldwide. We provide a selection of studies, both large-scale and local, documenting ephemeral and intermittent river regimes in regions with similar climate characteristics to the Gulf of Corinth.

Region		**Study**
Europe		(Sauquet et al., 2020, 2021)
	Greece	(Tzoraki et al., 2013) (Diakakis, 2012) (Ntigkakis et al., 2020; Varlas et al., 2018)
	Italy	(Piras et al., 2016)
	Spain	(Hooke, 2019) (del Moral et al., 2020)
Global	USA	(Hayden et al., 2021) (Sauquet et al., 2021)
	Australia	(Sauquet et al., 2021)

	Namibia	(Normandin et al., 2022)

Table S2. Compilation of studies documenting modern fluvial systems with similar discharge regimes and hydroclimates to those observed in the Gulf of Corinth, Greece.

S3: Köppen-Geiger climate zones

Climate change not only causes enhanced storminess, but aridification is increasing the area of global landscape that is potentially intermittency-dominated, as dry and arid regions are the most likely to host intermittent river systems (Sauquet et al., 2021). An active research challenge is projecting how climate zones may change due to global warming (e.g., Beck et al., 2018; Rohli et al., 2015) and research suggests up to a $1.6x10^6$ km^2 increase in arid landscape by 2100 (Rohli et al., 2015), with significant implications for global landscape sensitivity to climate change. Table S1 lists Köppen-Geiger climate zones, with those most likely to host intermittent systems, and those highlighted in Figure S1, in bold. Maps (Figure S1) show the regions expected (based on the dataset of Rohli et al. (2015) to be dry and arid in the near future.

1st	**2nd**	**3rd**
A (tropical)	f (rainforest) m (monsoon) w (savanna, dry winter) s (savanna, dry summer)	
B (dry)	**W (arid desert)** **S (semi-arid or steppe)**	**h (hot)** **k (cold)**
C (temperate)	w (dry winter) f (no dry season) **s (dry summer)**	**a (hot summer)** **b (warm summer)** c (cold summer)
D (continental)	w (dry winter) f (no dry season) s (dry summer)	a (hot summer) b (warm summer) c (cold summer) d (very cold winter)
E (polar)		T (tundra) F (ice cap)

Table S3. Köppen-Geiger climate zones, where the bold text indicates the zones highlighted in Fig S1.

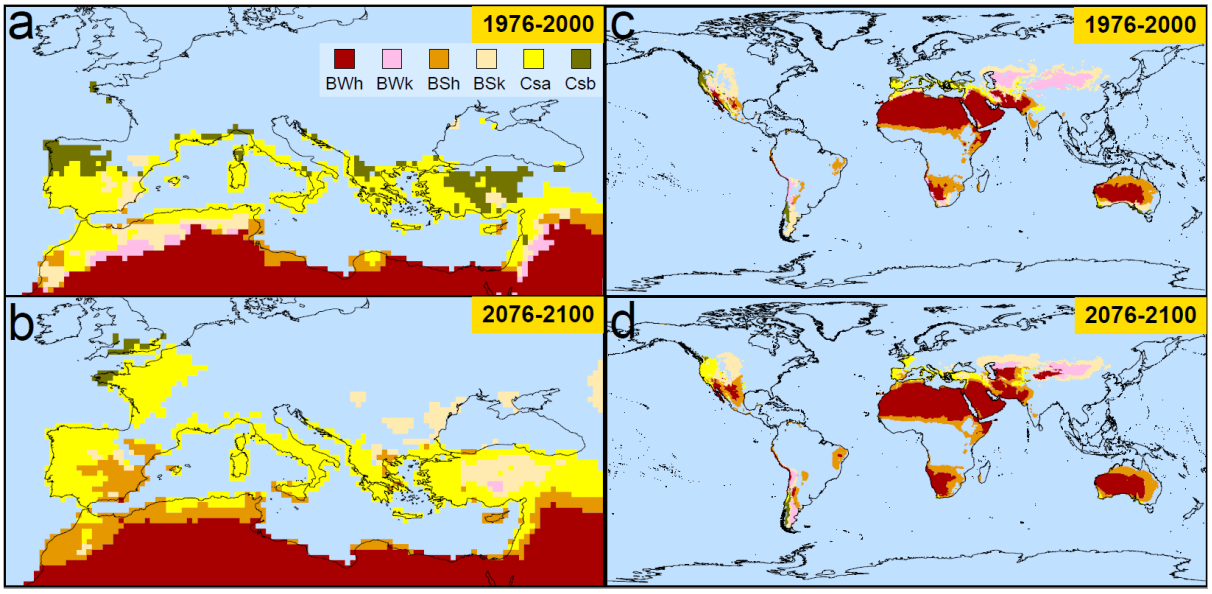

Fig S1. The dry and arid Koppen-Geiger climate zones in the Mediterranean (a, b) and the rest of the world (c, d), for 1976-2000 (a, c) and projected for 2076-2100 (b, d), based on the dataset of Rohli et al. (2015). These changes suggest that a growing area of land will become more sensitive to extreme precipitation by the end of the century.

S4. Extended methodology

S4.1. Estimating bankfull flow

In order to establish the bankfull sediment transport capacity of active ephemeral rivers in the Gulf of Corinth, it was necessary to estimate the bankfull flow depth in the field. We assume that the bedload grain-size distribution and indicators of maximum flow depth both represent the most recent geomorphically significant flow event, as our measurements by necessity describe the most recent flow event that transported bedload. Watkins et al. (2019) demonstrated by comparing Wolman point count results to full-weighted grain-size distributions for these rivers that the surface grain-size distribution is a good approximation of the average grain-size up to 1 m below the surface. In any case, it is true that more recent events may have reduced the measured bedload grain-size by adding smaller grains. This simply means that our estimates of bankfull sediment transport capacity are minima, and our intermittency factors are conservative maxima.

Two main indicators of flow depth were used: firstly, where channel banks were well-developed, bank geometry was sufficient to delineate the maximum water depth in bankfull conditions. Secondly, where banks were less well developed, the deepest recent flow event could be estimated using the maximum height of plant debris deposited on the river banks and amongst riparian vegetation. These methods have been tested in this region by Watkins et al, (2019) and Zondervan et al. (2020). The depth was measured using a Haglof Geo Laser Range Finder, in addition to the bankfull width, and slope. Bedload grain-size was determined using the Wolman point count method.

S4.2. The DV approach

To calculate intermittency, a catchment-basin volume (CBV) approach and a delta volume (DV) approach were used. The DV approach used a simplified model of delta volume based on seismic

sections from across the Gulf of Corinth. Topset length was measured from satellite imagery, and foreset depth was measured based on bathymetric data. These were transformed into a 3D shape representing delta volume by the model in Figure S2.

This shape is described by first estimating a delta cross-sectional area, A_1:

$$A_1 = A_0 - A_2$$

where

$$A_0 = \frac{d(r + r_1)}{2}$$

$$A_2 = \frac{r_1 d}{2}$$

$$r_1 = \frac{d \sin y}{\sin x}$$

and r is the length of the delta topset, d is the depth to the base of the foreset, x is 35° and y is 55°. This cross-section is used to estimate a volume (V_d) with a plan that is equivalent to that of a semi-circular prism, which has 79% the volume of a rectangular prism of the same dimensions.

$$V_d = 0.79(2rA_1)$$

This formula simplifies to

$$V_d = 0.79r^2 d$$

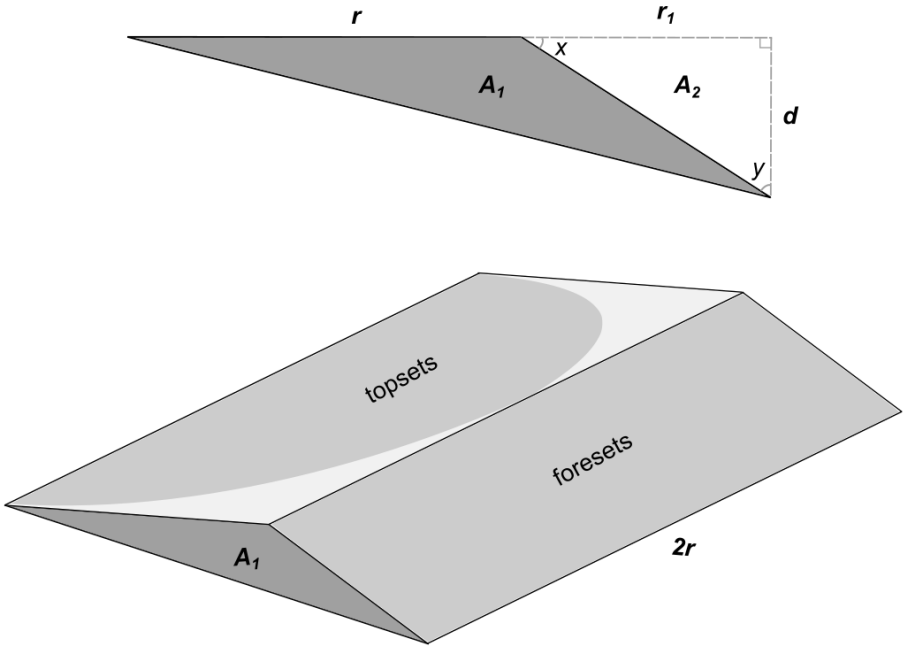

Figure S2: Simple model used in the Delta Volume approach, where r is the length of subaerial topsets, and d is the vertical depth to the bottomsets.

S4.3. The CBV approach

The CBV approach utilises BQART, a global multiregressional empirical model to estimate suspended sediment load (Q_s) based on 488 rivers (Syvitski & Milliman, 2007). Watkins et al. (2019) showed that the BQART model applied to the active channels in the Gulf of Corinth can predict Holocene sediment volumes to within a factor of 1.6 of those reconstructed from seismic data within the basin, meaning we can reasonably compare modern and Holocene sedimentary systems. Watkins et al. (2019) used this method to estimate suspended sediment load for each catchment. Therefore, to predict bedload flux, an assumption must be made on the ratio of bedload to total sediment flux (R_{bt}). In the preliminary intermittency calculations of Watkins (2019), a bedload fraction (R_{bt}) of 35% of total sediment yield was estimated based on an analogous system (Pratt-Sitaula et al., 2004).

The ratio of bedload to total sediment load is highly variable, and depends on climate, sediment supply, and discharge regime among many other factors. A literature survey of rivers in similar hydroclimates yielded R_{bt} values between 1 and 50% (Alexandrov et al., 2009; Avgeris et al., 2022; R. Batalla et al., 2005; R. J. Batalla, 1997; Karalis et al., 2022; Martín-Vide et al., 1999; Quintana-Seguí et al., 2011; Reid et al., 1998; Schick & Lekach, 1993; Turowski et al., 2010), with a preferred value between 20 and 30%.

To account for this uncertainty, we conducted an alternative analysis of the volumes of deltas on the rift margins and fine-grained basin-floor sediment from seismic data. The bulk basin R_{bt} was estimated by dividing the total volume of rift-margin coarse sediment stored in deltas by the total volume of Holocene sediment in the basin, estimated from seismic data (Watkins et al., 2019). This direct estimation of R_{bt} within the basin yielded a value of 0.25. We therefore present intermittency results using both R_{bt} = 0.25 and 0.35. All uncertainty has been propagated through calculations using Monte Carlo simulations, and the range of results are shown in Fig. 2 and the Supplementary Materials.

S4.4. Flood dataset

In order to contextualise intermittency calculations with real precipitation and flood events, historical data were compiled on significant events within 50 km of the study area from the same period as the precipitation time series presented in Fig. 3 in the main text.

Start date			Location	Rainfall duration, h	Return (y) assuming I_f = 4.67x10^{-4}	Max total rainfall, mm	Max 1-h rainfall, mm/h	Max discharge, m^3/s	No. fatalities	References
y	m	d								
2008	11	17	Rafina	7	2.5	49.3	23.7	22.3		1
2009	10	25	Rafina	15	5.4	31.4	16.8	29.7		1
2009	11	3	Rafina	10	3.6	36	16	22		1
2009	12	11	Rafina	11	3.9	84.6	18.6	25		1
2011	1	2	Rafina	8	2.9	32	16.8	17.3		1
2011	2	3	Rafina	39	13.9	148.6	12.2	79.7		1
2011	2	24	Rafina	19	6.8	92.2	26	37.9		1
2012	2	6	Rafina	11	3.9	48.6	21.2	38		1
2012	11	29	Rafina	8	2.9	54.4	37	24.4		1
2012	12	29	Rafina	18	6.4	209	27	37.3		1
2013	1	16	Rafina	4	1.4	20.8	15	16.6		1
2013	2	22	Rafina	18	6.4	138.8	39.4	152.8	1	2
2015	1	31	Sperchios	22	7.9	59				3, 4
2015	10	22	Med.	9	3.2	135			5	2

2017	11	13	Mandra, Attica	5	1.8	300	140	115	24	1-6
2018	9	28	Med.	24	8.6	138			4	2, 3

Table S4: Recent historical data on the most significant floods within 50 km of study area from 2000 – 2021. ([1]CRED, 2023; [2]Giannaros et al., 2020; [3]Ntigkakis et al., 2020; [4]Papagiannaki et al., 2022; [5]Psomiadis et al., 2020; [6]Varlas et al., 2018)

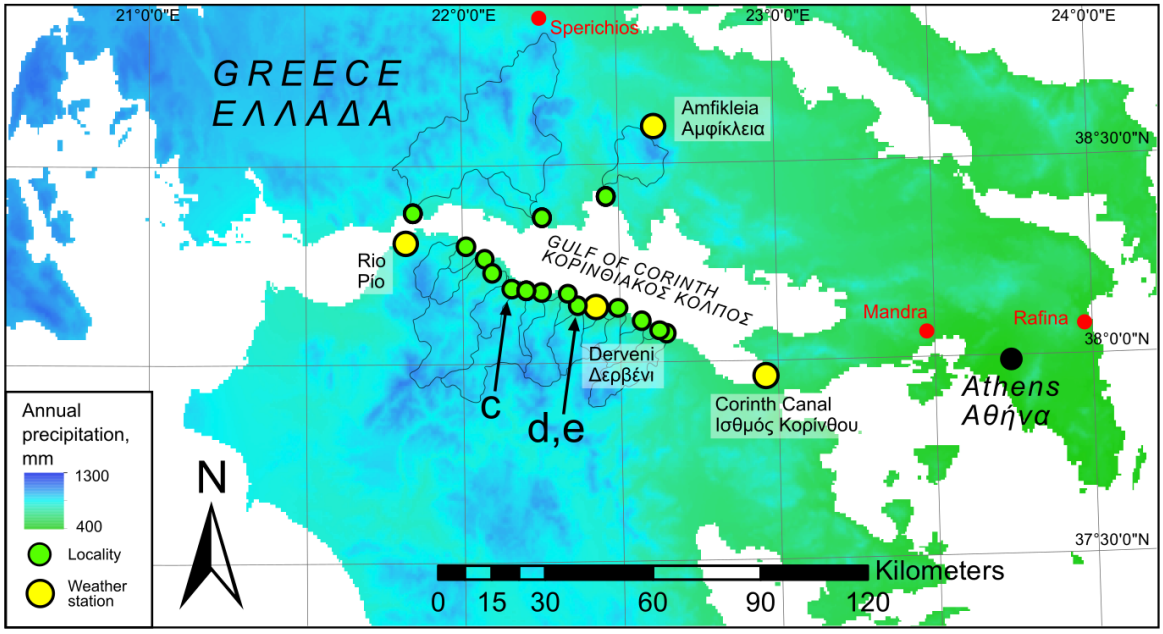

Fig S3. Map of the Gulf of Corinth, where red locations indicate the locations of studied precipitation and discharge dynamics in Table S4, used to inform estimates of recurrence intervals in analysis (see main text)

S4.5. Precipitation analysis

A simple scaling of compiled daily rainfall data in the Gulf of Corinth is used to illustrate the changes to sediment transport in the near future as a consequence of climate change. Figure 3c in the main text demonstrates that increasing all extreme precipitation by 20% (based on a literature review shown in Table S1) results in a 100% increase in the number of threshold-surpassing events within the 11-year time-series used. Figure S3 presents two alternative transformations applied to the same dataset.

In (a), events > 41.7 mm/d (= 50/1.2) are increased by 20% such that all extreme events (> 50 mm/d) have increased magnitude and frequency, resulting in the number of events surpassing each threshold to more-than double. The MAP increases by 2.5% (36 mm/a, i.e., there is no change to the mean within typical uncertainties), and the total volume of the 11-year hydrograph increases by 15%. In (b), events > 50 mm/d are increased by 20%, causing the number of events surpassing the 99.95% threshold to double, but those passing the 50 mm/d threshold to stay the same, as this generates a gap in the hydrograph between 50 and 60 mm/d. This approach increases the MAP by 1.5% and adds 9% to the total volume of the hydrograph. In (c), the entire hydrograph has been scaled up by 20%. This results in the same change in threshold-surpassing events as in (a), but increases both the MAP and the volume of the hydrograph by 20%.

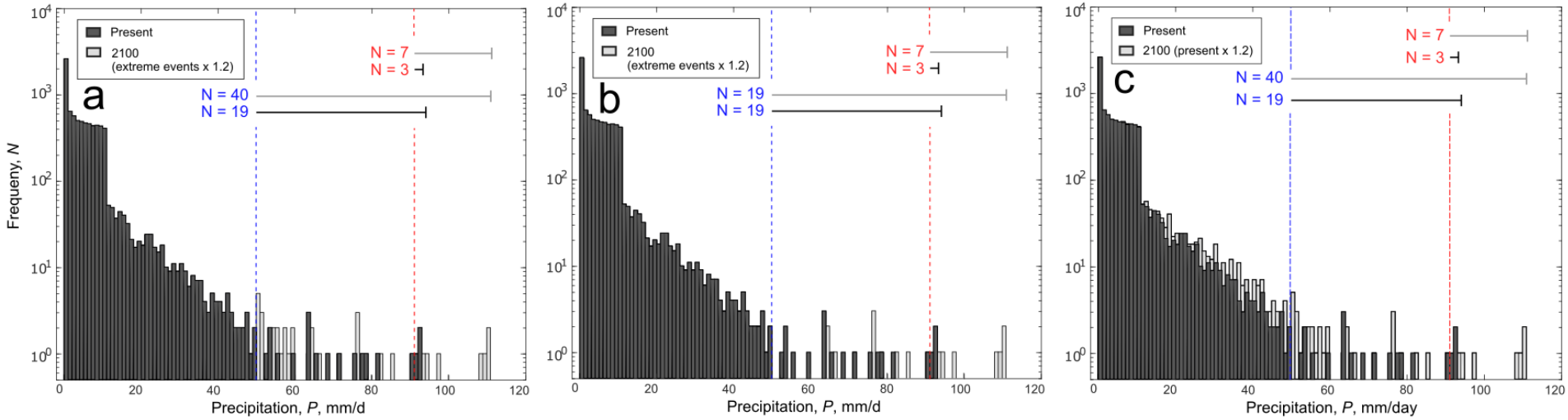
a
b
c
Present
2100
(extreme events x 1.2)
2100 (present x 1.2)
N = 7
N = 3
N = 40
N = 19
Frequeny, N
Precipitation, P, mm/d
Precipitation, P, mm/day

Fig. S4. Three approaches to scaling precipitation distributions acquired from four weather stations around the study area, in order to illustrate the effect of climate change on the number of threshold-surpassing events: (a) scaling the distribution above 41.7 mm/d by a factor of 1.2, in order to preserve the extreme events between 50 mm/d and 60 mm/d (=50*1.2); (b) scaling the distribution above 50 mm/d by a factor of 1.2; and (c) scaling the entire distribution by a factor of 1.2.

S4.6. Further datasets

A number of seismic reflection datasets were used in this study and the work of (Watkins, 2019; Watkins et al., 2019, 2020): (Leeder et al., 2002, 2005; Lykousis et al., 2007; Taylor et al., 2011; Zelt et al., 2004; McNeill et al., 2005; Bell et al., 2008).

The bathymetric models of Nixon et al. (2016) were used in the DV approach, based on the following datasets: (McNeill et al., 2005; Sakellariou et al., 2007; Taylor et al., 2011).

S5. Extended intermittency results

The intermittency factor results described in the main text can be trusted to reflect climate and precipitation patterns, as intermittency factor does not vary predictably with other geomorphic variables. Table S5 and Figure S5 demonstrate the random correlation between intermittency factor and catchment area, sediment flux, slope, and median grain-size.

	DV		**CBV 0.25**		**CBV 0.35**	
	Best fit	r^2	Best fit	r^2	Best fit	r^2
Catchment area vs I_f	y = 8E+09x + 1E+08	0.0037	y = 3E+11x + 2E+07	0.272	y = 2E+11x + 2E+07	0.272
Q_t vs I_f	y = -3E+06x + 61493	0.0059	y = -1E+07x + 64133	0.0096	y = -1E+07x + 64133	0.0096
S vs I_f	y = -4.3546x + 0.0459	0.0884	y = -15.874x + 0.0467	0.0748	y = -11.339x + 0.0467	0.0748
D_{50} vs I_f	y = 0.1251x + 0.0303	0.0008	y = 2.2657x + 0.0295	0.0129	y = 1.6169x + 0.0295	0.0129

Table S5: Results of regression between intermittency factor with channel/catchment variables across the Gulf of Corinth.

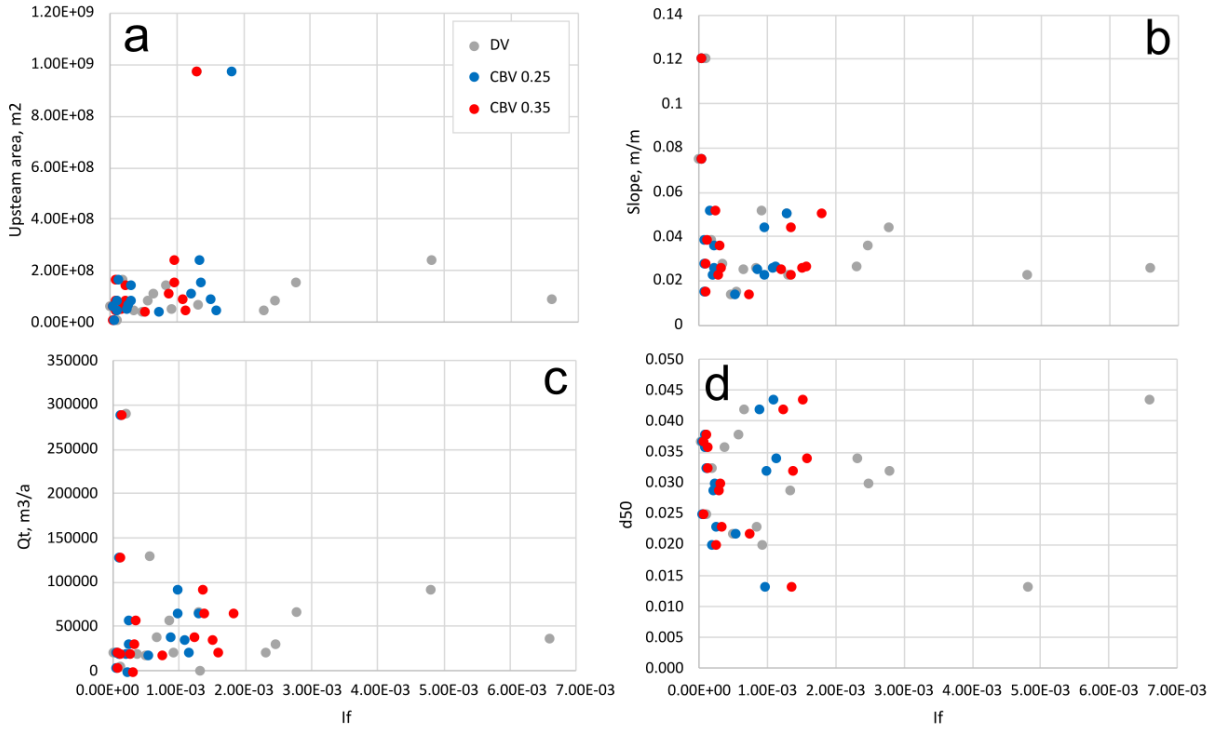

Fig S5: Scatter plots of intermittency factor on the x-axes and channel/catchment variables on the y-axes across the Gulf of Corinth.

Figure S6 displays the full range of intermittency factor results for each of the three approaches, at each locality, ordered clockwise around the Gulf. Uncertainties were determined using Monte Carlo propagation, displayed in full in Fig S6.

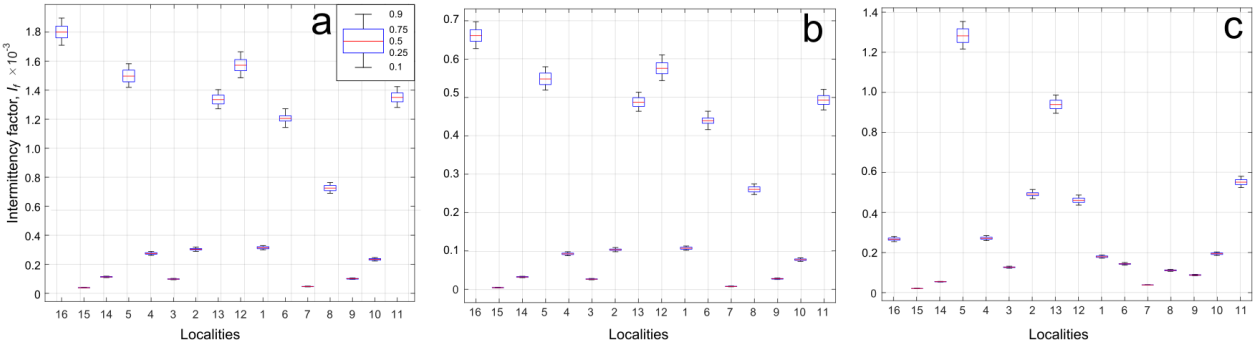

Fig S6: Boxplots of intermittency factor results for each locality (1-16), for (a) the CBV approach with $R_{bt} = 0.35$; (b) the CBV approach with $R_{bt} = 0.25$, and; (c) the DV approach.

REFERENCES

Alexandrov, Y., Cohen, H., Laronne, J. B., & Reid, I. (2009). Suspended sediment load, bed load, and dissolved load yields from a semiarid drainage basin: A 15-year study. *Water Resources Research*, *45*(8). https://doi.org/10.1029/2008WR007314

Arnone, E., Pumo, D., Viola, F., Noto, L. V., & La Loggia, G. (2013). Rainfall statistics changes in Sicily. *Hydrology and Earth System Sciences*, *17*(7), 2449–2458. https://doi.org/10.5194/hess-17-2449-2013

Avgeris, L., Kaffas, K., & Hrissanthou, V. (2022). Comparison between Calculation and Measurement of Total Sediment Load: Application to Streams of NE Greece. *Geosciences*, *12*(2), 91. https://doi.org/10.3390/geosciences12020091

Batalla, R., Garcia, C., & Balasch, J. (2005). Total sediment load in a Mediterranean mountainous catchment (the Ribera Salada River, Catalan Pre-Pyrenees, NE Spain). *Zeitschrift Für Geomorphologie*, *49*, 495. https://doi.org/10.1127/zfg/49/2005/495

Batalla, R. J. (1997). Evaluating Bed-material Transport Equations using Field Measurements in a Sandy Gravel-bed Stream, Arbúcies River, NE Spain. *Earth Surface Processes and Landforms*, *22*(2), 121–130. https://doi.org/10.1002/(SICI)1096-9837(199702)22:2<121::AID-ESP671>3.0.CO;2-7

Beck, H. E., Zimmermann, N. E., McVicar, T. R., Vergopolan, N., Berg, A., & Wood, E. F. (2018). Present and future Köppen-Geiger climate classification maps at 1-km resolution. *Scientific Data*, *5*(1), 180214. https://doi.org/10.1038/sdata.2018.214

Bell, R. E., McNeill, L. C., Bull, J. M., & Henstock, T. J. (2008). Evolution of the offshore western Gulf of Corinth. *GSA Bulletin*, *120*(1–2), 156–178. https://doi.org/10.1130/B26212.1

CRED. (2023). *EM_DAT, UCLouvain, Bussels* [dataset]. www.emdat.be

del Moral, A., Llasat, M. del C., & Rigo, T. (2020). Connecting flash flood events with radar-derived convective storm characteristics on the northwestern Mediterranean coast: Knowing the present for better future scenarios adaptation. *Atmospheric Research*, *238*, 104863. https://doi.org/10.1016/j.atmosres.2020.104863

Diakakis, M. (2012). Rainfall thresholds for flood triggering. The case of Marathonas in Greece. *Natural Hazards*, *60*(3), 789–800. https://doi.org/10.1007/s11069-011-9904-7

Fang, G., Yang, J., Li, Z., Chen, Y., Duan, W., Amory, C., & De Maeyer, P. (2022). Shifting in the global flood timing. *Scientific Reports*, *12*(1), 18853. https://doi.org/10.1038/s41598-022-23748-y

Giannakopoulos, C., Kostopoulou, E., Varotsos, K. V., Tziotziou, K., & Plitharas, A. (2011). An integrated assessment of climate change impacts for Greece in the near future. *Regional Environmental Change*, *11*(4), 829–843. https://doi.org/10.1007/s10113-011-0219-8

Giannaros, C., Kotroni, V., Lagouvardos, K., Oikonomou, C., Haralambous, H., & Papagiannaki, K. (2020). Hydrometeorological and Socio-Economic Impact Assessment of Stream Flooding in Southeast Mediterranean: The Case of Rafina Catchment (Attica, Greece). *Water*, *12*(9), 2426. https://doi.org/10.3390/w12092426

Goubanova, K., & Li, L. (2007). Extremes in temperature and precipitation around the Mediterranean basin in an ensemble of future climate scenario simulations. *Global and Planetary Change - GLOBAL PLANET CHANGE*, *57*, 27–42. https://doi.org/10.1016/j.gloplacha.2006.11.012

Hayden, A. T., Lamb, M. P., & McElroy, B. J. (2021). Constraining the Timespan of Fluvial Activity From the Intermittency of Sediment Transport on Earth and Mars. *Geophysical Research Letters*, *48*(16). https://doi.org/10.1029/2021GL092598

He, Y., Wang, Q., Xu, Y., Li, Z., Yuan, J., Lu, M., & Lin, Z. (2022). Climate change increased the compound extreme precipitation-flood events in a representative watershed of the Yangtze River Delta, China. *Stochastic Environmental Research and Risk Assessment*, *36*(11), 3803–3818. https://doi.org/10.1007/s00477-022-02229-8

Hooke, J. M. (2019). Extreme sediment fluxes in a dryland flash flood. *Scientific Reports*, *9*(1), 1686. https://doi.org/10.1038/s41598-019-38537-3

Karalis, S., Karymbalis, E., & Tsanakas, K. (2022). Estimating total sediment transport in a small, mountainous Mediterranean river: The case of Vouraikos River, NW Peloponnese, Greece. *Zeitschrift Für Geomorphologie*, 279–294. https://doi.org/10.1127/zfg/2021/0719

Leeder, M. R., Collier, R. E. Ll., Abdul Aziz, L. H., Trout, M., Ferentinos, G., Papatheodorou, G., & Lyberis, E. (2002). Tectono-sedimentary processes along an active marine/lacustrine half-graben margin: Alkyonides Gulf, E. Gulf of Corinth, Greece. *Basin Research*, *14*(1), 25–41. https://doi.org/10.1046/j.1365-2117.2002.00164.x

Leeder, M. R., Portman, C., Andrews, J. E., Collier, R. E. Ll., Finch, E., Gawthorpe, R. L., McNeill, L. C., Pérez-Arlucea, M., & Rowe, P. (2005). Normal faulting and crustal deformation, Alkyonides Gulf and Perachora peninsula, eastern Gulf of Corinth rift, Greece. *Journal of the Geological Society*, *162*(3), 549–561. https://doi.org/10.1144/0016-764904-075

Lykousis, V., Sakellariou, D., Moretti, I., & Kaberi, H. (2007). Late Quaternary basin evolution of the Gulf of Corinth: Sequence stratigraphy, sedimentation, fault–slip and subsidence rates. *Tectonophysics*, *440*, 29–51. https://doi.org/10.1016/j.tecto.2006.11.007

Martín-Vide, J. P., Niñerola, D., Bateman, A., Navarro, A., & Velasco, E. (1999). Runoff and sediment transport in a torrential ephemeral stream of the Mediterranean coast. *Journal of Hydrology*, *225*(3), 118–129. https://doi.org/10.1016/S0022-1694(99)00134-1

McNeill, L. C., Cotterill, C. J., Henstock, T. J., Bull, J. M., Stefatos, A., Collier, R. E. Ll., Papatheoderou, G., Ferentinos, G., & Hicks, S. E. (2005). Active faulting within the offshore western Gulf of Corinth, Greece: Implications for models of continental rift deformation. *Geology*, *33*(4), 241–244. https://doi.org/10.1130/G21127.1

Meresa, H., Tischbein, B., & Mekonnen, T. (2022). Climate change impact on extreme precipitation and peak flood magnitude and frequency: Observations from CMIP6 and hydrological models. *Natural Hazards*, *111*(3), 2649–2679. https://doi.org/10.1007/s11069-021-05152-3

Miranda, J. D., Armas, C., Padilla, F. M., & Pugnaire, F. I. (2011). Climatic change and rainfall patterns: Effects on semi-arid plant communities of the Iberian Southeast. *Journal of Arid Environments*, *75*(12), 1302–1309. https://doi.org/10.1016/j.jaridenv.2011.04.022

Nixon, C. W., McNeill, L. C., Bull, J. M., Bell, R. E., Gawthorpe, R. L., Henstock, T. J., Christodoulou, D., Ford, M., Taylor, B., Sakellariou, D., Ferentinos, G., Papatheodorou,

G., Leeder, M. R., Collier, R. E. LI., Goodliffe, A. M., Sachpazi, M., & Kranis, H. (2016). Rapid spatiotemporal variations in rift structure during development of the Corinth Rift, central Greece. *Tectonics*, *35*(5), 1225–1248. https://doi.org/10.1002/2015TC004026

Normandin, C., Paillou, P., Lopez, S., Marais, E., & Scipal, K. (2022). Monitoring the Dynamics of Ephemeral Rivers from Space: An Example of the Kuiseb River in Namibia. *Water*, *14*(19), Article 19. https://doi.org/10.3390/w14193142

Ntigkakis, C., Nezi, M., & Efstratiadis, A. (2020). Post-extraction of flood hydrographs under limited and heterogeneous information: Case study of Western Attica event, November 2017. *European Geosciences Union General Assembly 2020*. https://doi.org/egusphere-egu2020-18262

Papagiannaki, K., Petrucci, O., Diakakis, M., Kotroni, V., Aceto, L., Bianchi, C., Brázdil, R., Gelabert, M. G., Inbar, M., Kahraman, A., Kılıç, Ö., Krahn, A., Kreibich, H., Llasat, M. C., Llasat-Botija, M., Macdonald, N., de Brito, M. M., Mercuri, M., Pereira, S., … Zêzere, J. L. (2022). Developing a large-scale dataset of flood fatalities for territories in the Euro-Mediterranean region, FFEM-DB. *Scientific Data*, *9*(1), Article 1. https://doi.org/10.1038/s41597-022-01273-x

Piras, M., Mascaro, G., Deidda, R., & Vivoni, E. R. (2016). Impacts of climate change on precipitation and discharge extremes through the use of statistical downscaling approaches in a Mediterranean basin. *Science of The Total Environment*, *543*, 952–964. https://doi.org/10.1016/j.scitotenv.2015.06.088

Pratt-Sitaula, B., Burbank, D. W., Heimsath, A., & Ojha, T. (2004). Landscape disequilibrium on 1000–10,000 year scales Marsyandi River, Nepal, central Himalaya. *Geomorphology*, *58*(1–4), 223–241. https://doi.org/10.1016/j.geomorph.2003.07.002

Psomiadis, E., Diakakis, M., & Soulis, K. X. (2020). Combining SAR and Optical Earth Observation with Hydraulic Simulation for Flood Mapping and Impact Assessment. *Remote Sensing*, *12*(23), Article 23. https://doi.org/10.3390/rs12233980

Quintana-Seguí, P., Habets, F., & Martin, E. (2011). Comparison of past and future Mediterranean high and low extremes of precipitation and river flow projected using different statistical

downscaling methods. *Natural Hazards and Earth System Sciences*, *11*(5), 1411–1432. https://doi.org/10.5194/nhess-11-1411-2011

Reid, I., Laronne, J. B., & Powell, D. M. (1998). Flash-flood and bedload dynamics of desert gravel-bed streams. *Hydrological Processes*, *12*(4), 543–557. https://doi.org/10.1002/(SICI)1099-1085(19980330)12:4<543::AID-HYP593>3.0.CO;2-C

Rohli, R. V., Andrew Joyner, T., Reynolds, S. J., Shaw, C., & Vázquez, J. R. (2015). Globally Extended Köppen–Geiger climate classification and temporal shifts in terrestrial climatic types. *Physical Geography*, *36*(2), 142–157. https://doi.org/10.1080/02723646.2015.1016382

Sahabi-Abed, S., Ayugi, B. O., & Selmane, A. N.-E.-I. (2023). Spatiotemporal projections of extreme precipitation over Algeria based on CMIP6 global climate models. *Modeling Earth Systems and Environment*. https://doi.org/10.1007/s40808-023-01716-3

Sakellariou, D., Lykousis, V., Alexandri, S., Kaberi, H., Rousakis, G., Nomikou, P., Georgiou, P., & Ballas, D. (2007). Faulting, seismic-stratigraphic architecture and Late Quaternary evolution of the Gulf of Alkyonides Basin–East Gulf of Corinth, Central Greece. *Basin Research*, *19*(2), 273–295. https://doi.org/10.1111/j.1365-2117.2007.00322.x

Sauquet, E., Shanafield, M., Hammond, J. C., Sefton, C., Leigh, C., & Datry, T. (2021). Classification and trends in intermittent river flow regimes in Australia, northwestern Europe and USA: A global perspective. *Journal of Hydrology*, *597*, 126170. https://doi.org/10.1016/j.jhydrol.2021.126170

Sauquet, E., van Meerveld, I., Gallart, F., Sefton, C., Parry, S., Gauster, T., Laaha, G., Alves, M. H., Arnaud, P., Banasik, K., Beaufort, A., Bezdan, A., Datry, T., De Girolamo, A. M., Dörflinger, G., Elçi, A., Engeland, K., Estrany, J., Fialho, A., … Żelazny, M. (2020). *A catalogue of European intermittent rivers and ephemeral streams*. Zenodo. https://doi.org/10.5281/ZENODO.3763419

Schick, A., & Lekach, J. (1993). An evaluation of two ten-year sediment budgets, Nahal Yael, Israel. *Physical Geography*, *14*, 225–238. https://doi.org/10.1080/02723646.1993.10642477

Syvitski, J. P. M., & Milliman, J. D. (2007). *Geology, Geography, and Humans Battle for Dominance over the Delivery of Fluvial Sediment to the Coastal Ocean | The Journal of Geology: Vol 115, No 1*. *115*(1), 1–19.

Taylor, B., Weiss, J. R., Goodliffe, A. M., Sachpazi, M., Laigle, M., & Hirn, A. (2011). The structures, stratigraphy and evolution of the Gulf of Corinth rift, Greece. *Geophysical Journal International*, *185*(3), 1189–1219. https://doi.org/10.1111/j.1365-246X.2011.05014.x

Tramblay, Y., & Somot, S. (2018). Future evolution of extreme precipitation in the Mediterranean. *Climatic Change*, *151*(2), 289–302. https://doi.org/10.1007/s10584-018-2300-5

Turowski, J. M., Rickenmann, D., & Dadson, S. J. (2010). The partitioning of the total sediment load of a river into suspended load and bedload: A review of empirical data: The partitioning of sediment load. *Sedimentology*, *57*(4), 1126–1146. https://doi.org/10.1111/j.1365-3091.2009.01140.x

Tzoraki, O., Cooper, D., Kjeldsen, T., Nikolaidis, N. P., Gamvroudis, C., Froebrich, J., Querner, E., Gallart, F., & Karalemas, N. (2013). Flood generation and classification of a semi-arid intermittent flow watershed: Evrotas river. *International Journal of River Basin Management*, *11*(1), 77–92. https://doi.org/10.1080/15715124.2013.768623

Varlas, G., Anagnostou, M. N., Spyrou, C., Papadopoulos, A., Kalogiros, J., Mentzafou, A., Michaelides, S., Baltas, E., Karymbalis, E., & Katsafados, P. (2018). A Multi-Platform Hydrometeorological Analysis of the Flash Flood Event of 15 November 2017 in Attica, Greece. *Remote Sensing*, *11*(1), 45. https://doi.org/10.3390/rs11010045

Watkins, S. E. (2019). *Linking source and sink in an active rift: Quantifying controls on sediment export and depositional stratigraphy in the Gulf of Corinth, central Greece*. Imperial College London.

Watkins, S. E., Whittaker, A. C., Bell, R. E., Brooke, S. A. S., Ganti, V., Gawthorpe, R. L., McNeill, L. C., & Nixon, C. W. (2020). Straight from the source's mouth: Controls on field-constrained sediment export across the entire active Corinth Rift, central Greece. *Basin Research*, *32*(6), 1600–1625. https://doi.org/10.1111/bre.12444

Watkins, S. E., Whittaker, A. C., Bell, R. E., McNeill, L. C., Gawthorpe, R. L., Brooke, S. A. S., & Nixon, C. W. (2019). Are landscapes buffered to high-frequency climate change? A comparison of sediment fluxes and depositional volumes in the Corinth Rift, central Greece, over the past 130 k.y. *GSA Bulletin*, *131*(3–4), 372–388. https://doi.org/10.1130/B31953.1

Westra, S., Fowler, H. J., Evans, J. P., Alexander, L. V., Berg, P., Johnson, F., Kendon, E. J., Lenderink, G., & Roberts, N. M. (2014). Future changes to the intensity and frequency of short-duration extreme rainfall: FUTURE INTENSITY OF SUB-DAILY RAINFALL. *Reviews of Geophysics*, *52*(3), 522–555. https://doi.org/10.1002/2014RG000464

Zelt, B. C., Taylor, B., Weiss, J. R., Goodliffe, A. M., Sachpazi, M., & Hirn, A. (2004). Streamer tomography velocity models for the Gulf of Corinth and Gulf of Itea, Greece. *Geophysical Journal International*, *159*(1), 333–346. https://doi.org/10.1111/j.1365-246X.2004.02388.x

Zondervan, J. R., Whittaker, A. C., Bell, R. E., Watkins, S. E., Brooke, S. A. S., & Hann, M. G. (2020). New constraints on bedrock erodibility and landscape response times upstream of an active fault. *Geomorphology*, *351*, 106937. https://doi.org/10.1016/j.geomorph.2019.106937